

Research Article

Anti-cancer activity of crude Slrp protein conjugated mesoporous silica nanoparticles in HeLa Cell Lines: An *in vitro* approach

Shiva Prasad Panjala

Department of Genetics and Biotechnology, University College of Science, Osmania University, Hyderabad-500007 (Telangana), India; Food Chemistry Division, National Institute of Nutrition, Indian Council of Medical Research, Hyderabad-500007 (Telangana), India

Satyanarayana Swamy Vyshnava

Department of Biotechnology, University College of Science, Sri Krishnadevaraya University, Anantapuramu-515003 (Andhra Pradesh), India; Department of Microbiology, Keshav Memorial Institute of Commerce and Sciences, Narayanguda, Hyderabad-500029, (Telangana), India

Swathi Banapuram

Clinical Division, National Institute of Nutrition, ICMR, Hyderabad-500007 (Telangana), India

Vihari Vasikarla

University of California, Data Science, At Halicioglu Data Science Institute, La Jolla -92037 (San Diego), United States of America

Paramasivam Kameshpandian

DMI St. John The Baptist University, Lilongwe Campus P.O. Box 2398, Area 4 (Lilongwe Malawi), Central Africa

Muralidhara Rao Dowlathabad

Department of Biotechnology, University College of Science, Sri Krishnadevaraya University, Anantapuramu-515003 (Andhra Pradesh), India

Roja Rani Anupalli*

Department of Genetics and Biotechnology, University College of Science, Osmania University, Hyderabad-500007 (Telangana), India

*Corresponding author: E-mail: anupallirr@gmail.com

Article Info

<https://doi.org/10.31018/jans.v16i1.5285>

Received: November 20, 2023

Revised: February 26, 2024

Accepted: March 3, 2024

How to Cite

Panjala, S.P. *et al.* (2024). Anti-cancer activity of crude Slrp protein conjugated mesoporous silica nanoparticles in HeLa Cell Lines: An *in vitro* approach. *Journal of Applied and Natural Science*, 16(1), 364 - 377. <https://doi.org/10.31018/jans.v16i1.5285>

Abstract

Microbial based therapeutics for cancer have gained a significant interest in recent decades. The present study relies on the synthesis, analysis, and conjugation of Salmonella Leucine-rich Proteins (SlrP) with mesoporous silica nanoparticles (MSN^N) to evaluate their potential anticancer activity. The SlrP proteins were effectively produced and isolated from *Salmonella enterica* using Tryptic Soy Broth (TSB), and the subsequent SDS-PAGE analysis verified the presence of a band at around 72 KDa. The MSN synthesis yielded particles with an average diameter of 68.05±0.87 nm and a pore diameter of 7.1 nm. In addition, we synthesized MSN^{MPA} and then conjugated them with SlrP. Characterization studies confirmed the effective conjugation. The cytotoxicity evaluation conducted on HeLa cells revealed no substantial modification in cell viability upon treatment with MSN alone. Nevertheless, when MSN^{MPA/SlrP} was done, it demonstrated significant cytotoxic properties, as evidenced by an IC₅₀ value of 10 µg/mL. The results indicate that SlrP-conjugated MSN (MSN^{MPA/SlrP}) could be utilized as promising nanocarriers for delivering anticancer proteins.

Keywords: Anti-cancer activity, Bio-conjugations, Bacterial Proteins, Mesoporous silica, Nanoparticles

INTRODUCTION

Cancer, a relatively intricate and complicated ailment, is a significant factor in global mortality (Bray *et al.* 2018). Despite significant progress in cancer therapy,

the pursuit of more efficient and less harmful treatments remains a fundamental objective in oncology research (Pucci, Martinelli and Ciofani 2019, Kuznetsov, Clairambault and Volpert 2021). An emerging approach in this field is, harnessing proteins produced

from bacteria as anti-cancer agents (Shelburne et al. 2014, Zugazagoitia et al. 2016). Considering their evolutionary interactions with eukaryotic cells, bacterial proteins and peptides offer an intrinsic capacity to selectively target physiological processes, rendering them promising candidates for cancer therapy (Nutti et al. 2017, Cubillos-Ruiz et al. 2021).

Throughout the past studies, it has been extensively reported that bacteria have a tendency to specifically infect tumor tissues, a behavior that has been observed for more than a century (Rook and Dalgleish 2011, Dzutsev et al. 2017, Huang et al. 2021). In recent decades many research groups have been studying the potential of bacterial proteins in cancer therapies due to their distinct activity (Forbes 2010, Roy and Trinchieri 2017, Wong and Yu 2019, Cani 2018). Specific bacterial proteins have been discovered to trigger programmed cell death in cancer cells, hinder the formation of new blood vessels, and regulate the immune response in a way that promotes the depletion of the size of tumors (Huang et al., 2021; Lugano et al., 2020; Sedighi et al., 2019; Liang et al. 2019). Three categories of bacteria have been investigated for their potential as agents that can combat cancer. Class I includes obligatory anaerobes such as *Bifidobacteria Sp.* (*B. longum*, *B. adolescentis*, *B. infantis*), which are Gram-positive bacteria renowned for their probiotic characteristics, and they possess an oncolytic function (Wei et al., 2008; Dailey et al., 2021).

Class II includes facultative intracellular bacteria, such as *Salmonella Sp.* (*S. typhimurium*, *S. choleraesuis*) and *Listeria Sp.* (*L. monocytogenes*), as well as *E. coli*. These bacteria possess the ability to attack tumors of various sizes selectively and hold promise as carriers for vaccines (Sedighi et al., 2019; Toussaint et al., 2013; Kalia et al., 2022; Guimalda et al., 2012). *Salmonella Sp.* Strains exhibit a substantial ratio of 1000:1 between tumors and normal tissue. Nevertheless, the cell wall components of these organisms can induce an immune response, and there are safety problems associated with administering them in high quantities (Barrow, 2007; Hurley et al., 2014). Class III comprises exclusively anaerobic bacteria, such as *Clostridium Sp.*, which can be further classified as proteolytic (*C. sporogenes*) and saccharolytic (*C. novyi*, *C. butyricum*, *C. acetobutylicum*, *C. oncolyticum*, *C. beijerinckii*) (Van Mellaert, 2006; Zargar, 2014; Jafari et al., 2012). These bacteria that create spores are durable and exhibit significant oncolytic capabilities. However, they can only colonise big tumors and can be pathogenic in certain strains (Zygouropoulou et al., 2019).

Leschner et al., 2009 group provide insights of bacterium *Salmonella Sp.* have been thoroughly investigated as tumour invasion of *Salmonella enterica* (Leschner et al., 2009). While the *Salmonella* leucine-rich repeat protein (SlrP) is notable among its assortment of pro-

teins as reported by the research group (Figueroa-Bossi et al. 2001; Ramos-Morales, 2012; Haraga, 2005; Ehrbar et al., 2003). The distinctive interactions of SlrP with eukaryotic cells, including its tendency to disrupt host cellular processes, indicate a promising potential for its utilization in cancer treatment (Lu, 2015 ; Layton and Galyov, 2007).

Nevertheless, although bacterial proteins present a new and innovative method for cancer treatment, their instantaneous application is not devoid of obstacles (Liu et al., 2018; Albalawi et al., 2021; Martín et al. 2015). Observations have been made concerning aspects such as the possibility of causing an immune response, quick breakdown in the body's circulation, and unintended effects on nonspecific targets (Liu et al., 2018; Martín et al., 2015). In order to address these challenges, researchers utilize medication delivery techniques that rely on nanoparticles (Anchordoquy et al., 2017; Chenthamara et al., 2019). Out of the many different types of nanoparticles that have been investigated, mesoporous silica nanoparticles (MSNs) have received considerable interest (Kankala et al., 2019; Manzano and Vallet-Regí, 2020). MSN's are characterized by their non-toxic nature, biocompatibility, large surface area, adjustable pore size, and convenient ability to be modified with different functionalities (Florek et al., 2017; Ahmadi et al., 2022). Due to their distinctive characteristics, they are excellent vehicles for medicinal substances, ensuring precise delivery while reducing the occurrence of nonspecific adverse effects (Frickestein et al., 2021; Hossen et al., 2019; Farjadi-an et al., 2019).

The present study aimed to investigate the effectiveness of conjugation of SlrP with MSNs as a novel strategy for cancer treatment. The aim was to synthesize and analyze SlrP-conjugated MSNMPA (MSN^{MPA/SlrP}), assess their potential as anticancer agents *in-vitro*, specifically in their capacity to target and impede the proliferation of cancer cells. Furthermore, the study seeks to evaluate these linked nanoparticles' compatibility with potential toxicity to determine their safety for therapeutic applications.

MATERIALS AND METHODS

Chemicals and Reagents

Microbial media include Luria Bertani Broth (LB), Nutrient Broth (NB), Tryptone Soya Broth (TSB), Tryptone Soya Agar (TSA) were purchased from Loba Chem Pvt Ltd, India. Mammalian cell culture media include the Dulbecco's Modified Eagle Medium (DMEM), Fetal Bovine Serum (FBS), Penicillin:Streptomycin solution (Pen:Strep), trypsin-EDTA and 1X PBS solution was purchased from Himedia. Lysis buffer, Triton X-100, Protease inhibitor, Formaldehyde (HCHO), Cetyltrimethylammonium bromide (CTAB), Ammonium hydroxide

(NH₄OH), Tetraethyl orthosilicate (TEOS), Ethanol (EtOH), Methanol (MeOH), Propanol (PrOH), 1-ethyl-3-(3-dimethylaminopropyl) carbodiimide (EDC), N-hydroxy succinimide (NHS), 2-(N-morpholino) ethanesulfonic acid (MES) buffer and Acetone (Ac) organic solvent were purchased from Tokyo Chemicals Industry Pvt Ltd. Acrylamide (Acr), Bis-acrylamide (B-Acr), Sodium Dodecyl Sulfate (SDS), Tris (hydroxymethyl)aminomethane (Tris), β -mercapto-propionic acid (β -MPA) were purchased from Sigma-Aldrich, Ammonium Persulfate (APS), Tetramethylethylenediamine (TEMED), β -mercaptoethanol, Bromophenol Blue were purchased from Merck Chemical.

Bacterial culture and crude protein preparation

Salmonella enterica was obtained from "National Centre for Microbial Resource (NCMR), Pune, India. *S. enterica* standard strain (MCC 3910) is kept at 4°C on Nutrient Agar medium (NAM) slants, while glycerol stock is kept at -80°C. Throughout this study, *S. enterica* was maintained in a contamination free environment with proper ethical guidelines to be followed, to maintain the bacterial strain with proper microbial cultures and disposals. TSB was used as the growth medium for the bacterial culture of *S. enterica*. A solitary colony of *S. enterica*, obtained from a recently streaked agar plate, was introduced into TSB, LB and NB subjected to incubation at a temperature of 37°C, while continuously agitated at 200 rpm for overnight incubation. The culture was diluted into a fresh medium and allowed to develop until the optical density at 600 nm (OD₆₀₀) reached a value between 0.6 and 0.8, indicating the mid-logarithmic phase.

After the growth phase, the bacterial culture was subjected to centrifugation at a force of 4,000 rpm for 10 minutes at a temperature of 4°C to collect the cells. The resulting pellet was rinsed twice with cold 1X PBS. To extract SlrP, the pellet was mixed with a lysis buffer (50 mM Tris-HCl at pH 8.0, 150 mM NaCl) and 1% Triton X-100. The lysis buffer was further added with a protease inhibitor cocktail. The process of breaking down cells was accomplished by subjecting them to sonication while kept on ice. The sonication was performed with specific parameters: 10 cycles of 30 seconds of sonication followed by 30 seconds of rest, at an amplitude of 40%. After sonication, the lysate was subjected to centrifugation at a force of 12,000 rpm for 20 minutes at a temperature of 4°C to separate the cell debris.

The liquid portion, which included the unrefined protein extract, was subsequently analyzed using sodium dodecyl sulfate-polyacrylamide gel electrophoresis (SDS-PAGE). The gel slice was processed to extract the protein, which was then identified as the crude protein extract. To ensure extended preservation and future ex-

perimentation, portions of this extract were stored at a temperature of -80°C (Tsakalidou *et al.*, 1994; Costas 1995).

Synthesis of Mesoporous silica nanoparticles

The synthesis of MSN^N (MSNs with naked, unmodified surface) was based on the hydrothermal synthesis methods developed by Gu *et al.* (2012) with minor changes to the temperature and time variables for particle growth. Initially, 442 mL of deionized water was adjusted to a pH of 11 by introducing 10.8 g of NH₄OH, a solution containing 30% NH₃ by weight in water. Subsequently, 0.279 grams of CTAB was introduced into the HCHO solution with vigorous stirring. The temperature of the combination steadily increased to 50°C, simultaneously with an increase in the stirring speed. The outcome led to a reduction in the pH of the CTAB solution to 10.3. Once the solution had reached the ambient temperature, 1.394 mL of tetraethyl orthosilicate (TEOS) was added. Within a span of 120 seconds, the solution underwent a modest turbidity and the pH level dropped to 9.8, suggesting a fast hydrolysis of the silicate. Approximately 2 hours later, the pH rose to 10.6, possibly because of silica condensation. Following the completion of the previously mentioned procedure, the sample was further subjected to filtration and calcination. The formed MSN^N were collected in a centrifuge tube by using acidified methanol thrice the volume of the MSN^N solution, washed twice or thrice to remove any excess CTAB and formaldehyde. The precipitate after centrifugation (4000 rpm at Room temperature for 10 minutes) was collected dried, and the fine powder of MSN^N was stored at room temperature until further use. The purified MSN^N were characterized utilizing a wide range of techniques. The morphology and size of the nanoparticles were analyzed using Transmission Electron Microscopy (TEM) (ThermoFisher TALOS F200S) and Scanning Electron Microscopy (SEM) (TESCAN-MIRA 3-Quantax 200), to observe distinct and consistent structure. Atomic Force Microscopy (AFM) (Innova SPM) was used to find precise topographical data and validate the nanoparticles' surface roughness. The X-ray Diffraction (XRD) (Rigaku Smartlab) study was used to observe distinct peaks, providing evidence of the crystalline structure and purity of the produced MSNs. The optical properties were investigated using UV-visible absorbance spectroscopy and Fourier Transform Infrared Spectroscopy (FTIR) (Thermo Nicolet iS50), which will provide the existence of certain functional groups or sizes by unique absorption peaks. Dynamic Light Scattering (DLS) (Malvern Nano ZS) and Zeta potential measurements were used to determine the hydrodynamic diameter and surface charge of the nanoparticles in suspension, confirming their stability and uniform distribution.

Surface modification of Mesoporous silica nanoparticles

The MSN^N were further modified by incorporating a monodentate thiol ligand, specifically β -MPA, onto the surface to introduce a negative charge with the modified previously published protocol (Wang *et al.*, 2015; Vyshnava *et al.*, 2022a; Vyshnava *et al.*, 2020; Vyshnava *et al.*, 2022c). MSN^N were thoroughly cleaned by dispersing them in ethanol and subjected the mixture to ultrasonication bath for one hour. The surface contaminants were effectively eliminated through subsequent centrifugation and vacuum drying. To make the MSN^{MPA} surface ligand exchange, 50 mg of the purified particles were mixed with 10 mL of a freshly prepared solution containing 10 mM of β -MPA in dimethyl sulfoxide (DMSO), while maintaining inert conditions. Subsequently, the mixture was agitated for 24 hours at ambient temperature, facilitating the development of thiol-silica bonds due to the negative charge imparted to the MSN surface by the carboxylic acid group of β -MPA. The functionalized MSN^{MPA} were subjected to centrifugation and washed three times, alternating between DMSO and ethanol, to eliminate any excess β -MPA. The MSN^{MPA} product proceeded with vacuum drying and was analyzed using AFM, FTIR, DLS, and zeta potential procedures to confirm the successful binding of β -MPA to the MSNs, which possessed a negative charge.

Conjugation of Mesoporous silica nanoparticles with SirP protein

Further the MSN^{MPA} were allowed to conjugate with the crude SirP protein using EDC/NHS coupling chemistry MES buffer based on earlier established protocols (Vyshnava *et al.*, 2022b; Lin *et al.*, 2019). Initially, 10 mg of the MSN^{MPA} was evenly distributed in 5 mL of MES buffer (pH 6.0) to create a uniform mixture. Simultaneously, EDC and NHS were dissolved in MES buffer to achieve final concentrations of 10 mM and 5 mM, respectively. The EDC/NHS solution was slowly added to the MSN^{MPA} suspension while stirring continuously to activate the carboxylic acid groups on the β -MPA capped MSN^{MPA}. Following a 15-minute activation period, the excess EDC and NHS were removed using centrifugation of the MSN^{MPA} suspension (4000 rpm at 4°C for 15 minutes), and the resulting pellet was then re-suspended in a new MES buffer. Afterwards, a solution containing the SirP protein at a concentration of 1 μ g/mL was added to the activated MSN^{MPA} suspension. The combination was then stirred gently at a temperature of 4°C for a duration of 4 hours. This allowed for the formation of covalent bonds between the SirP protein, and the carboxylic groups present on the MSN^{MPA}. Ultimately, MSN^{MPA/SirP} were separated using centrifugation (4000 rpm at 4°C for 15 minutes), carefully rinsed with 1X PBS to eliminate any free protein in the

reaction solution, and then suspended again in 1X PBS and stored at -20°C for subsequent examination and analysis.

Cell culture

The DMEM, supplemented with 10% fetal bovine serum (FBS) and 1% antibiotic solution (10,000 units of Pen:Strep solution), was used to grow HeLa cells (Acquired from NCCS Pune, India). The cultures were kept in an incubator with humidity control, 5% CO₂ atmosphere, and a temperature setting of 37°C. A trypsin-EDTA buffer solution with a pH of 7.4 was used to facilitate cell dissociation, followed subsequent subculture the cells every two weeks for further experimentations.

Cytotoxicity of MSN^N and MSN^{MPA}

The MTT assay was used to assess the cytotoxic effects of MSN^N and MSN^{MPA} on HeLa cells. At first, HeLa cells were placed in 96-well microtiter plates (MTP) with a density of 1×10^5 cells per well and allowed to adhere overnight. The following cells were exposed to increasing doses of MSN^N and MSN^{MPA} (0, 20, 40, 60, 80, and 100 μ g/mL) in triplicate in their respective wells of MTP. The plates were there after placed in an incubator set at a temperature of 37°C and an environment containing 5% CO₂ for a period of 24 hours. Following the incubation period, the vitality of the cells was evaluated using the MTT assay, following established recommendations. The nanoparticles' cytotoxicity was measured by identifying the concentration at which 50% inhibition of cells occurred (IC₅₀).

Anticancer activity of MSN^{MPA/SirP}

This work extended the results obtained from evaluating the effects of MSN^N and MSN^{MPA} on HeLa cells by further investigating the anticancer activity of MSN^{MPA/SirP} (Cheng *et al.*, 2017). The HeLa cells were placed in 96-well plates with a concentration of 1×10^5 cells per well and allowed to settle for overnight. Subsequently, the cells were treated with increasing amounts of MSN^{MPA/SirP} (0, 0.1, 1.0, 10, 20, and 40 μ g/mL). The plates were placed in an incubator set at a temperature of 37°C and an environment with 5% CO₂ for 24 hours. Following the incubation period, the vitality of the cells was assessed using the MTT test in accordance with established guidelines. The nanoparticles' cytotoxicity was assessed by determining the IC₅₀ value, which corresponds to the concentration that causes a 50% reduction in cell viability.

Additionally, the Olympus inverted microscope was employed to examine the morphological changes in the HeLa cells. This examination aimed to assess the cell membrane's integrity and identify cellular bleeding caused due to MSN^{MPA/SirP} impact. We used 1mm coverslips on a 6 well plate. Each well was seeded with

the HeLa cells of 1×10^5 cells per well, followed by incubation for 24 hours to check the confluency of minimum 60 %. Later, based on the IC_{50} values from the previous cytotoxicity assay, the $MSN^{MPA/SirP}$ were added to the respective wells and allowed them to incubate for overnight. Various magnifications were utilized to observe and record a comprehensive perspective on cellular responses to the treatment. The MTT assay and morphological analysis combination provides a relative insight into the impacts of $MSN^{MPA/SirP}$ nanoparticles on HeLa cells.

RESULTS AND DISCUSSION

Crude SirP protein production and characterization

Salmonella enterica was effectively cultured in TSB broth with precise control over the parameters in our experiment. The bacterial culture's development was assessed by quantifying the optical density at 600 nm, where readings ranging from 0.6 to 0.8 indicated the successful attainment of the mid-logarithmic phase, as shown in the Supporting information Fig. S1. Following centrifugation and subsequent washing, the bacterial cells were lysed to extract the SirP in microgram (μ g) quantities, thus successfully accomplishing the primary goal of this study. As shown in Fig. 1(a), the crude protein SDS-PAGE data revealed the clear band at around 72 KDa, which corresponds to the established molecular weight for crude SirP proteins. This result was consistent with the earlier reports from Zouhir *et al.*, 2014; Bernal-Bayard, Cardenal-Munoz and Ramos-Morales, 2010, Cordero-Alba and Ramos-Morales, 2014). The yield of crude extract for triplicate experimentation was 3.9, 4.3, and 4.1 μ g of protein for 5mg of bacterial pellets. This steady exploration confirms the reliability and accuracy of our protein extraction approach.

After comparing TSB, NB and LB broth, as shown in Fig. 1(a), it was shown that the production of the SirP protein was noticeably greater in cultures cultivated in TSB. This observation indicates that TSB may create a more favorable environment for *S. enterica* to generate and concentrate the desired protein, making it the favored option for subsequent extraction (Observe the relative concentrations in Supporting information Fig. S1). The utilization of gel slicing and salting-out procedures enabled the retrieval of the crude state of the protein from several SDS-PAGE gels. An additional SDS-PAGE study, as shown in Fig. 1(b) provided further verification of the protein's existence in microgram quantities. It was maintained at extremely low temperatures of -80°C to maintain its stability and longevity to preserve the protein extract for future experimental objectives.

Synthesis and characterization MSN^N nanoparticles

The production of MSN^N was initially demonstrated by the appearance of a turbid white precipitate in the HCHO solution, a behavior that has been reported in previous investigations (Gu *et al.*, 2012). The link between the sizes of particles and pores in MSN and the concentration of the silica source, tetraethyl orthosilicate (TEOS), has been previously described (Gu *et al.*, 2012; Zhang *et al.*, 2011; Manzano and Vallet-Regí, 2020; Maggini *et al.*, 2016; Mohseni *et al.*, 2015). UV-Visible spectroscopy detected a distinct peak at 640 nm, as shown in Fig. 2(a), consistent with the distinctive pattern of silica nanoparticles observed in a previous report from Parasuraman *et al.* (2019). The morphology and size distribution of the MSN were examined in further detail using SEM results, as shown in Fig. 2(b), which confirmed the presence of spherical nanoparticles with noticeable pores, which aligns with

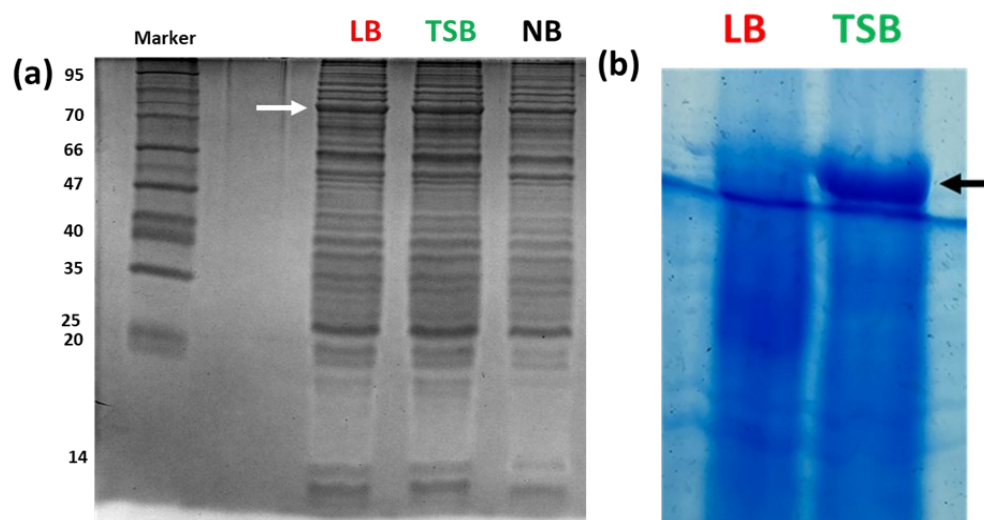


Fig. 1. SDS-PAGE Gel images of SirP crude protein run from *Salmonella enteric* (a) SirP crude protein yield with respective media including LB, TSB, and NB broth (b) Gel slicing and salting out the protein followed by protein run to check the weight of the protein in micrograms

previous reports (Zhang *et al.*, 2011; Gu *et al.*, 2012; Mohseni *et al.*, 2015; Hossen *et al.*, 2019). As shown in Fig. 2(c) and 2(d), TEM analysis revealed that the average particle size was 68.05 ± 0.87 nm, and the mean pore size was 7.1 nm. Further study with AFM, the particles exhibited distinct spherical shapes with a

uniform distribution. The particles also had a relatively rough surface due to the presence of pores, as depicted in Fig. 3(a). This observation was further confirmed by DLS, which revealed that the MSNN particles had a hydrodynamic size of 68 ± 0.8 nm, as shown in Fig. 3(b).

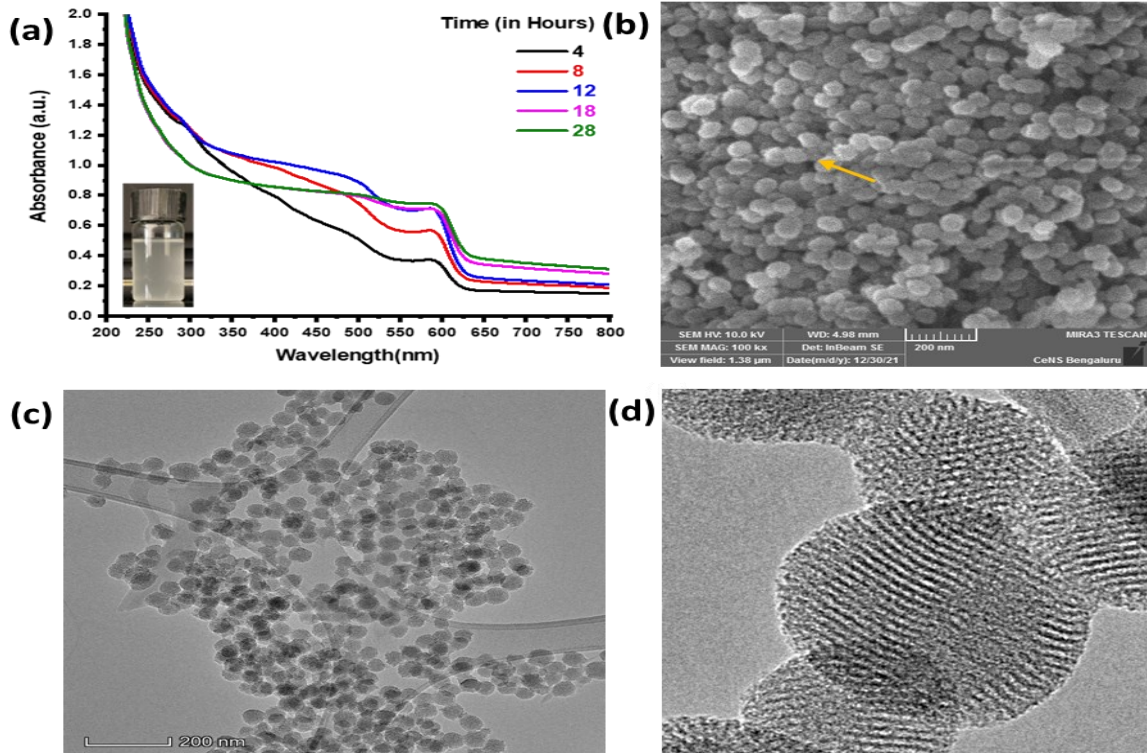


Fig. 2. Characterization of MSNN using (a) UV-Visible spectroscopy with the characteristic peak at 640nm on the absorbance spectrum, (b) Scanning electron microscopic image reveals the spherical morphology, (c & d) High resolution transmission electron microscopy showing crystal structure with specific d-spaces

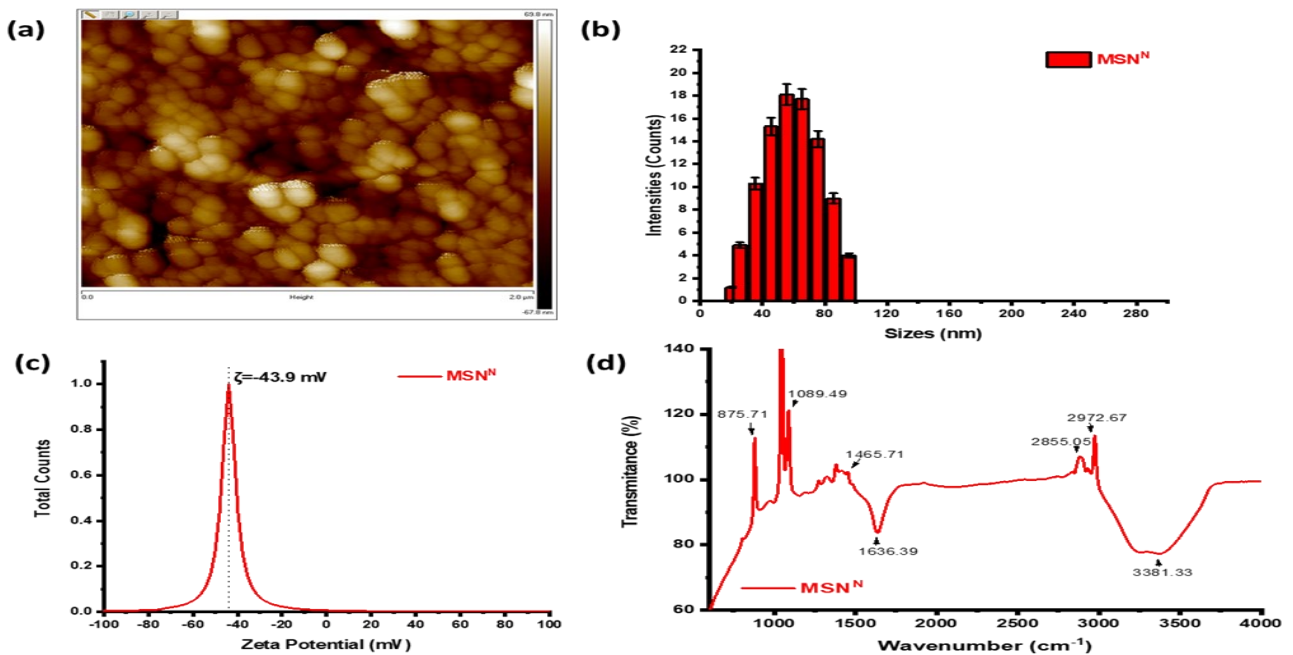


Fig. 3. Characterization of MSNN using (a) Atomic force microscopy with contact mode showing clear rough surface spherical nanoparticles, (b) Hydrodynamic size distribution using dynamic light scattering, (c) Zeta potential of the particles, (d) Fourier Transform Infrared Spectroscopy, peaks with distinctive peaks for surface functional groups

Additionally, the zeta potential measurements indicated a surface charge of approximately -43.9 mV as shown in Fig. 3(c), which is consistent with previous reports (Kaasalainen *et al.*, 2017; Kobler *et al.*, 2008). The distribution of functional groups was assessed using FTIR. Strong peaks were observed at wavenumbers 3381.33, 2972.67, 2855.05, 1636.39, 1465.71, 1089.49, and 875.71 cm^{-1} , which correspond to the -OH, -COO, -C=O, -N-H, and -CN peaks as observed in Fig. 3(d). These findings are consistent with previous results (Rameli *et al.*, 2018).

Ligand exchange and characterization MSN^{MPA} nanoparticles

Following the ligand exchange of the MSN^N, we assess the structural integrity of the MSN^N using X-ray Diffraction (XRD) analysis. The analysis shows a consistent amorphous pattern without any noticeable peaks, which is a characteristic feature of MSN and indicates the stability of the particles before (MSN^N) and after (MSN^{MPA}) ligand exchange as shown in Fig. 4(a) and (b) (Keshavarz and Ahmad 2013). The results obtained from AFM and DLS analyses confirmed a minimal increase in particle size, with an average diameter of approximately 69.77 ± 1.3 nm. The distribution of the particles was found to be uniform, as depicted in Fig. 5 (a) and 5(b). The Zeta potential, as presented in Fig. 5 (c), indicates a reduction in surface charge to -26.5 mV. The distinct peaks observed in the FTIR spectrum, spe-

cifically at wavenumbers 3352.63, 2980.98, 2897.88, 1392.40, 1243.59, and 1066.82 cm^{-1} , correspond to functional groups such as -OH, -COOH, -C=O, -C-C-, and -CN as shown in Fig. 5(d). The present study primarily utilize monodentate ligands, specifically β -MPA, for two primary goals: firstly, to augment the stability of the nanoparticles, and secondly, to offer the most advantageous negatively charged -COOH groups for subsequent conjugations. These findings agree with previous reports and indicate the successful transformation of the ligand, resulting in the presence of a negatively charged -COO- group (Gao *et al.*, 2021).

Bioconjugation of Mesoporous silica nanoparticles with SlrP

The above prepared MSN^{MPA} were further used to conjugate with crude SlrP using EDC/NHS coupling chemistry in the relatively suitable buffer MES. This observation is consistent with earlier investigations on nanoparticle-protein conjugation. The AFM scans confirmed these findings, revealing a surface covered with randomly threadlike structures, which are assumed to be dispersed SlrP protein molecules, as shown in Fig. 6 (a). The DLS results indicated a marginal augmentation in the hydrodynamic radius of the MSNs upon SlrP conjugation, implying the effective binding of the protein with a size distribution of 76 ± 3.2 nm as shown in Fig. 6 (b). The reduction in the negative charge of the MSNs, as determined by Zeta potential measurements, i.e.,

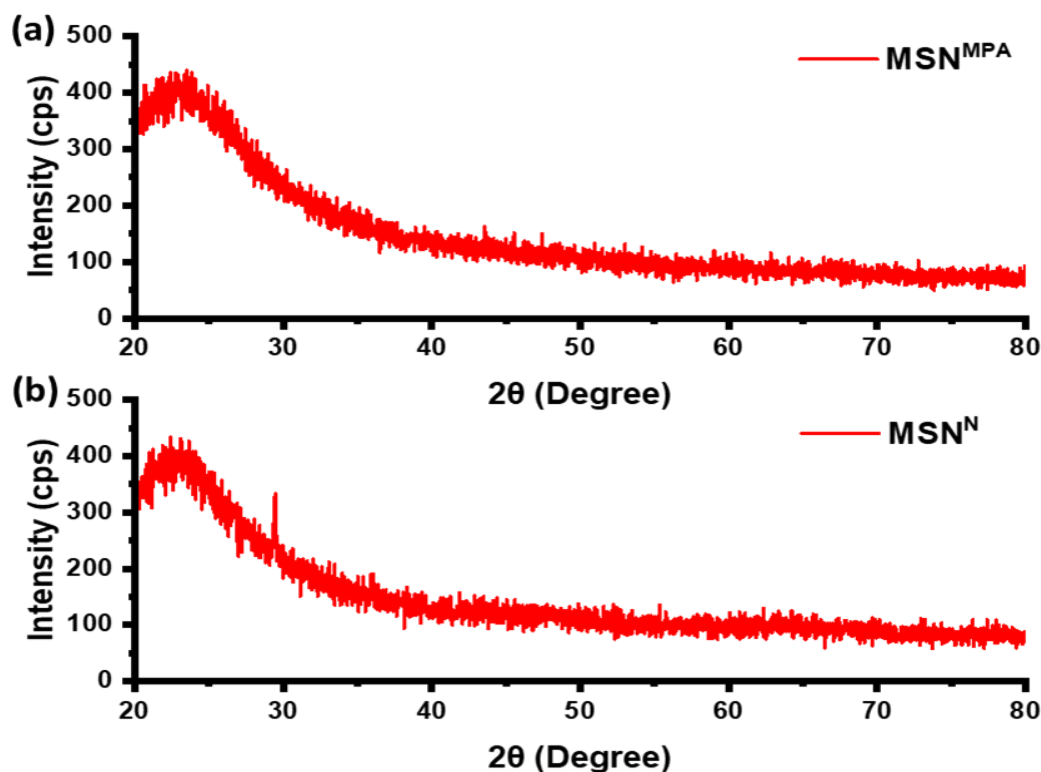


Fig. 4. X-ray diffraction spectrum of MSN^N and MSN^{MPA} with characteristic peak absence defines the amorphous nature of the particles

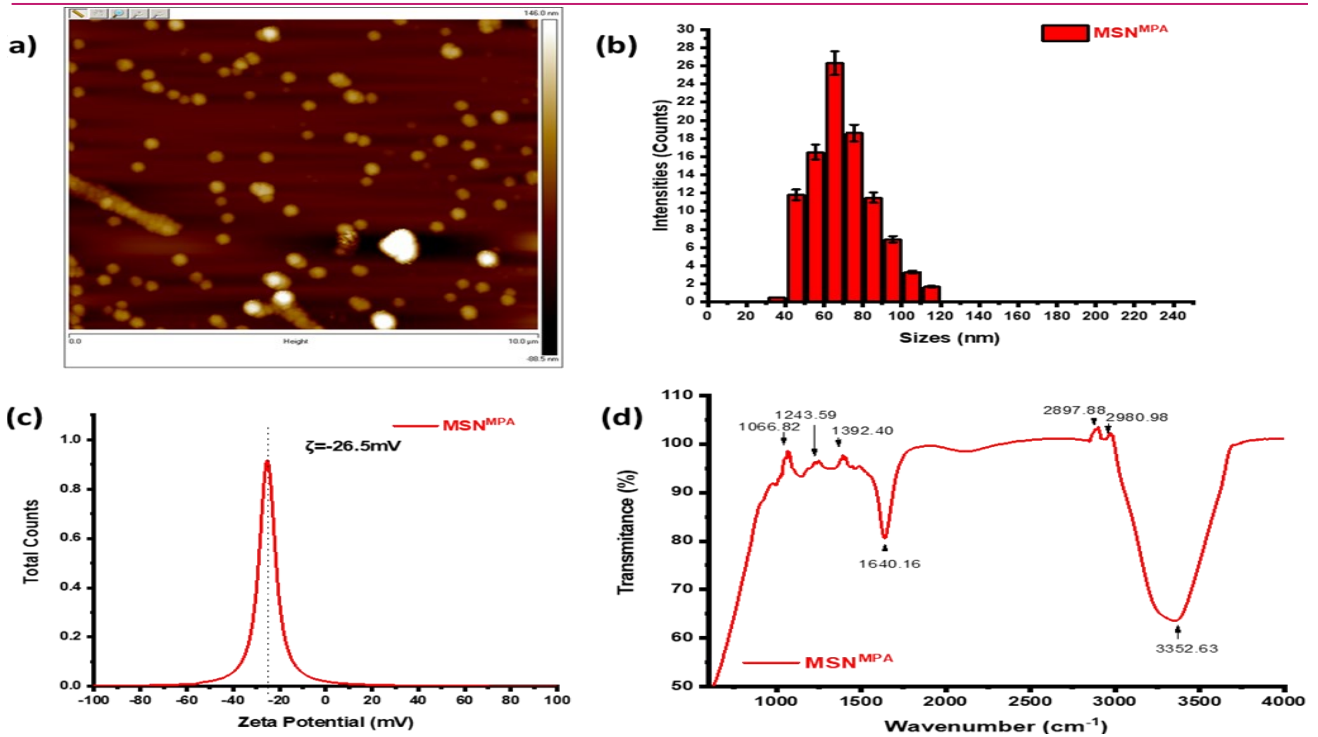


Fig. 5. Characterization of MSN^{MPA} using (a) Atomic force microscopy with contact mode showing clear rough surface spherical nanoparticles, (b) Hydrodynamic size distribution using dynamic light scattering, (c) Zeta potential of the particles, (d) Fourier Transform Infrared Spectroscopy peaks with distinctive peaks for surface functional groups

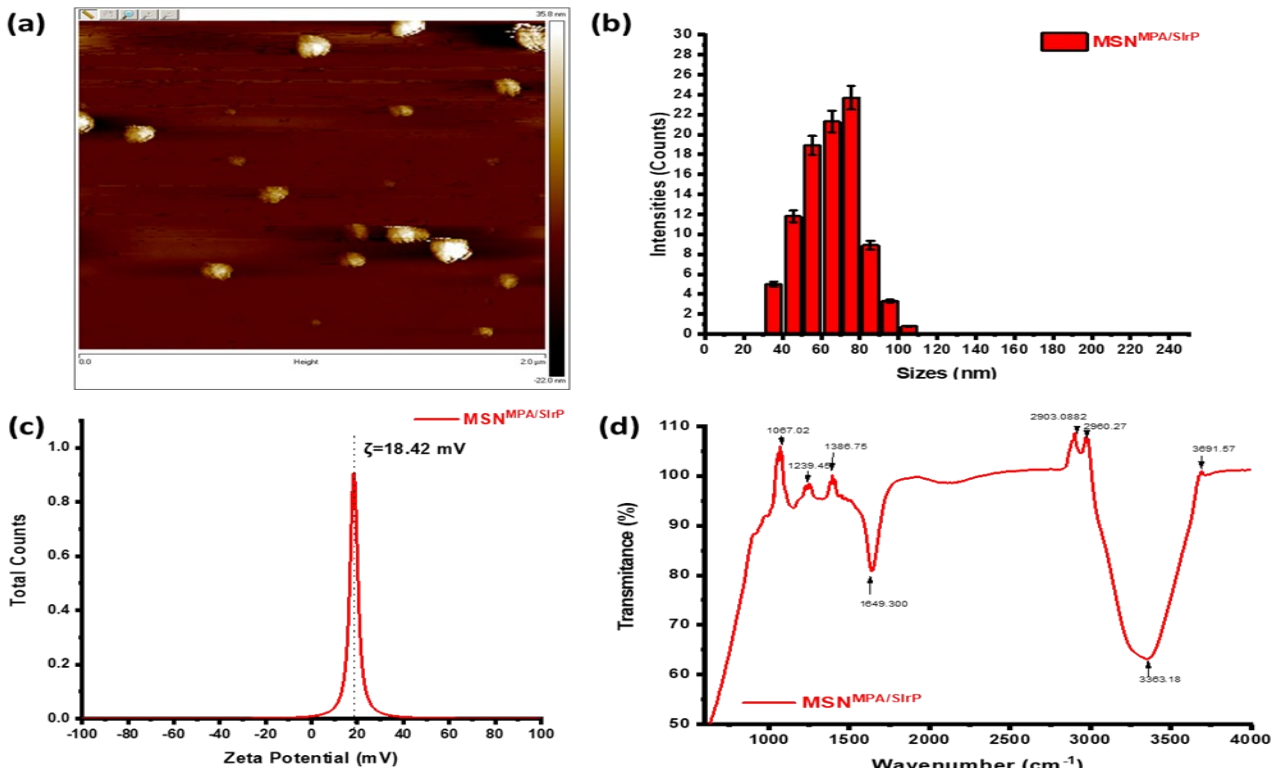


Fig. 6. Characterization of $MSN^{MPA/SirP}$ using (a) Atomic force microscopy with contact mode showing clear rough surface spherical nanoparticles, (b) Hydrodynamic size distribution using dynamic light scattering, (c) Zeta potential of the particles (d) Fourier Transform Infrared Spectroscopy peaks with distinctive peaks for surface functional groups

+18.42, indicates effective protein binding as shown in Fig. 6(c). FTIR spectroscopy provided additional verification of the conjugation, exhibiting distinctive peaks

which include 3691.57, 3363.18, 2960.27, 2903.08, 1649.30, 1386.75, 1239.45, and 1067.02 corresponding to -OH, -COOH, -C=O, -C-C-, -CN and -SH func-

tional groups, which are indicative of EDC/NHS coupling, which shows the effective binding of SlrP on MSN^{MPA} to form a functional MSN^{MPA/SlrP} as shown in Fig. 6(d). The prepared conjugates are stored at -20°C for further experimentation.

Cytotoxicity studies of MSN^N and MSN^{MPA}

Prior to investigating the anticancer efficacy of MSN^{MPA/SlrP}, the cytotoxicity of mesoporous silica nanoparticles, namely MSN^N and MSN^{MPA}, will be evaluated on HeLa cells. This establishes standard controls and ensures that any observed effects can be attributed to the therapeutic agent rather than a direct impact from the nanoparticles. Our findings showed that there was no significant change in the viability of HeLa cells after being incubated for 24 hours, even when exposed to high concentrations of respective MSN^N and MSN^{MPA}, up to 100 µg/mL and greater as shown in the as shown in Fig. 7(a). This observation highlighted the biocompatibility of MSN^N and MSN^{MPA}, with *in-vitro* studies consistent with previous research that found MSN nontoxic in cellular settings (Asefa and Tao,2012; Tang et al., 2012).

Anticancer activity SlrP Conjugated Mesoporous silica nanoparticles

Building on our initial findings, we undertook additional studies to assess the cytotoxic effects of MSN^{MPA} in combination with SlrP protein i.e., MSN^{MPA/SlrP} towards HeLa cell lines. In contrast to prior observations, we noted a substantial reduction in cell viability even at reduced concentrations of 50 µg/mL, exhibiting an exponential trend. The IC₅₀ value was found to be 10 µg/mL, suggesting a pronounced cytotoxic effect at relatively low concentrations as shown in Fig. 7(b). The cytotoxicity of both free SlrP and MSN^{MPA/SlrP} was evaluated to validate these findings. The IC₅₀ values were consistent, with SlrP showing concentrations of 50 µg/mL and for MSN^{MPA/SlrP} ≈50 µg/mL, respectively as depicted in Fig. 7(c). These results suggest that MSN^{MPA/SlrP} holds potential as an effective delivery system for anticancer proteins in *in vitro* cell culture experiments. Cellular morphology was assessed using an Olympus inverted microscope to substantiate further present cytotoxicity findings. Cells exposed to MSN^N and

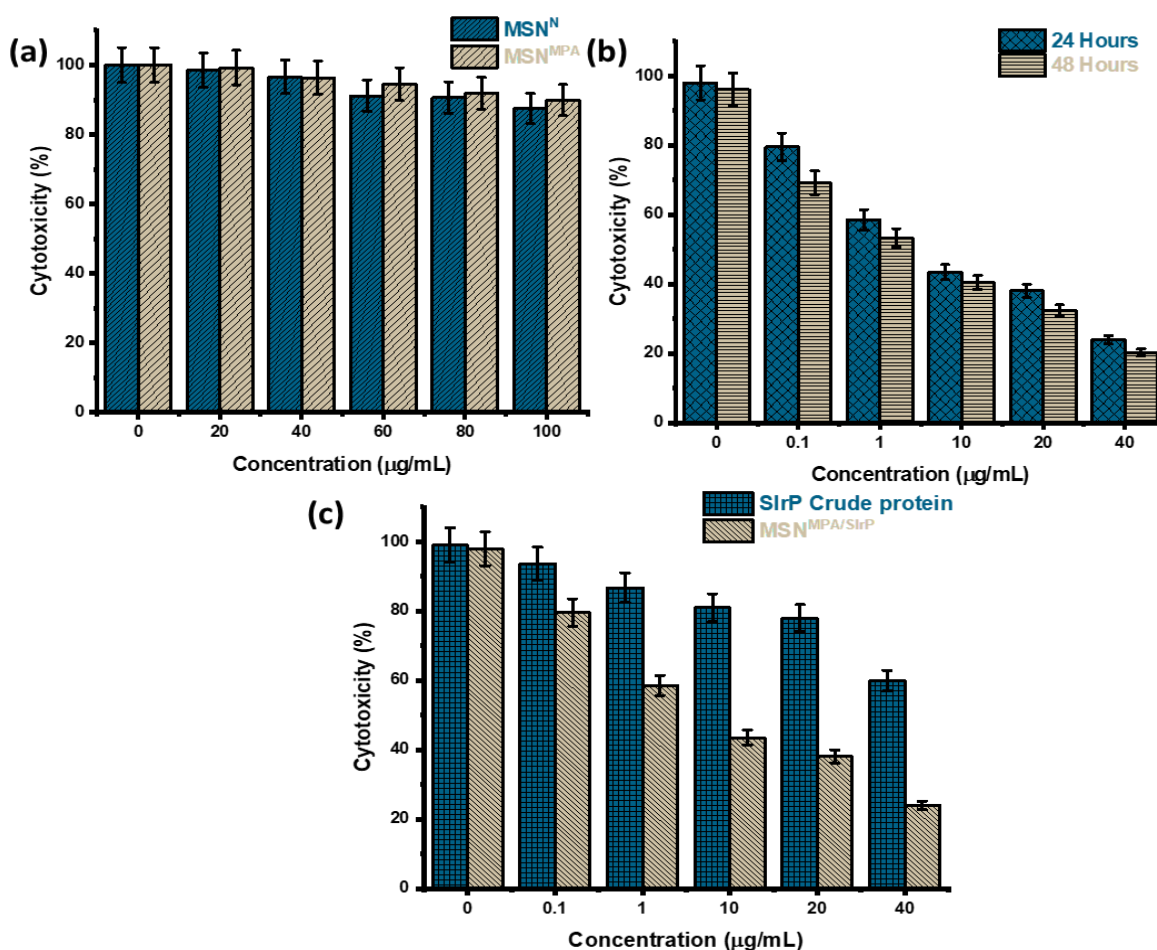


Fig. 7. Cytotoxicity studies of MSNs on the HeLa Cells (a) MSN^N and MSN^{MPA} toxicity studies with negligible cytotoxicity were observed (b) MSN^{MPA/SlrP} cytotoxicity was observed with significant decline in the viability in 24 hours followed by 48 hours (c) comparative estimation of native crude SlrP and MSN^{MPA/SlrP} with the reliable performance of the mesoporous particles in maintain the intact nature of the protein from cellular enzymes

MSN^{MPA} showed no significant morphological alterations, aligning with the observed lack of cytotoxicity as depicted in Fig. 8(a) and 8(b). Conversely, HeLa cells treated with MSN^{MPA/SirP} exhibited initial adherence issues, followed by detachment, cellular bleeding after 24 hours, and subsequent cell aggregation after 48 hours. These morphological observations, in conjunction with the cytotoxicity data, underscore the potential anti-

cancer properties of MSN^{MPA/SirP} complexes as shown in Fig. 9. The observed biocompatibility of MSN^N and MSN^{MPA} aligns with prior research underscoring the low toxicity of mesoporous silica nanoparticles (Braun *et al.*, 2018; Di Pasqua *et al.*, 2008; Jafari *et al.*, 2012; Jafari *et al.*, 2019). However, the MSN^{MPA/SirP} combination demonstrated cytotoxic potential, positioning it as a promising candidate for cancer therapy. The enhanced

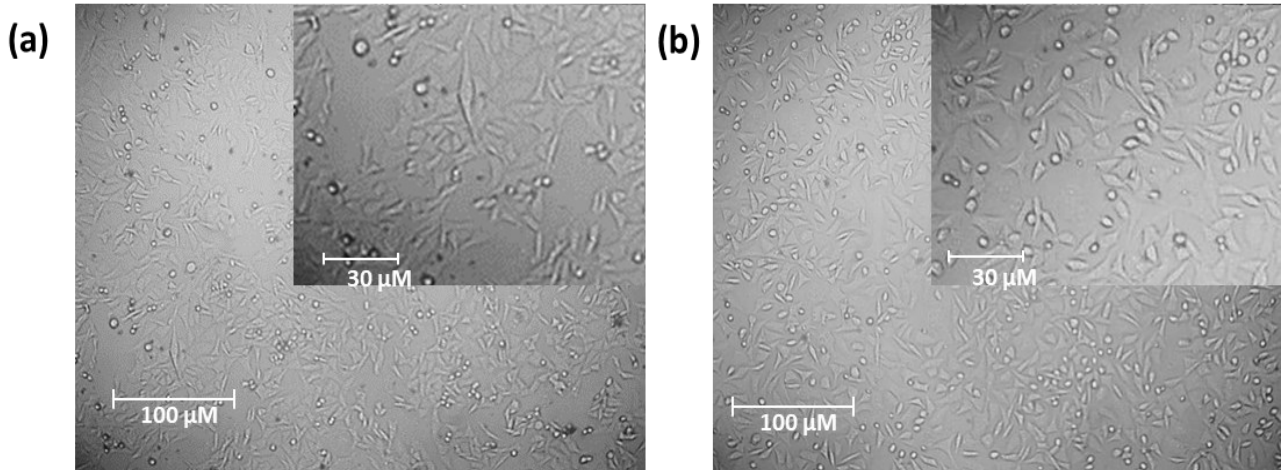


Fig. 8. Microscopic images of HeLa cells treated with (a) MSN^N, (b) MSN^{MPA} where negligible toxicity was observed, suggest the best biocompatibilities for the MSN^N and MSN^{MPA}

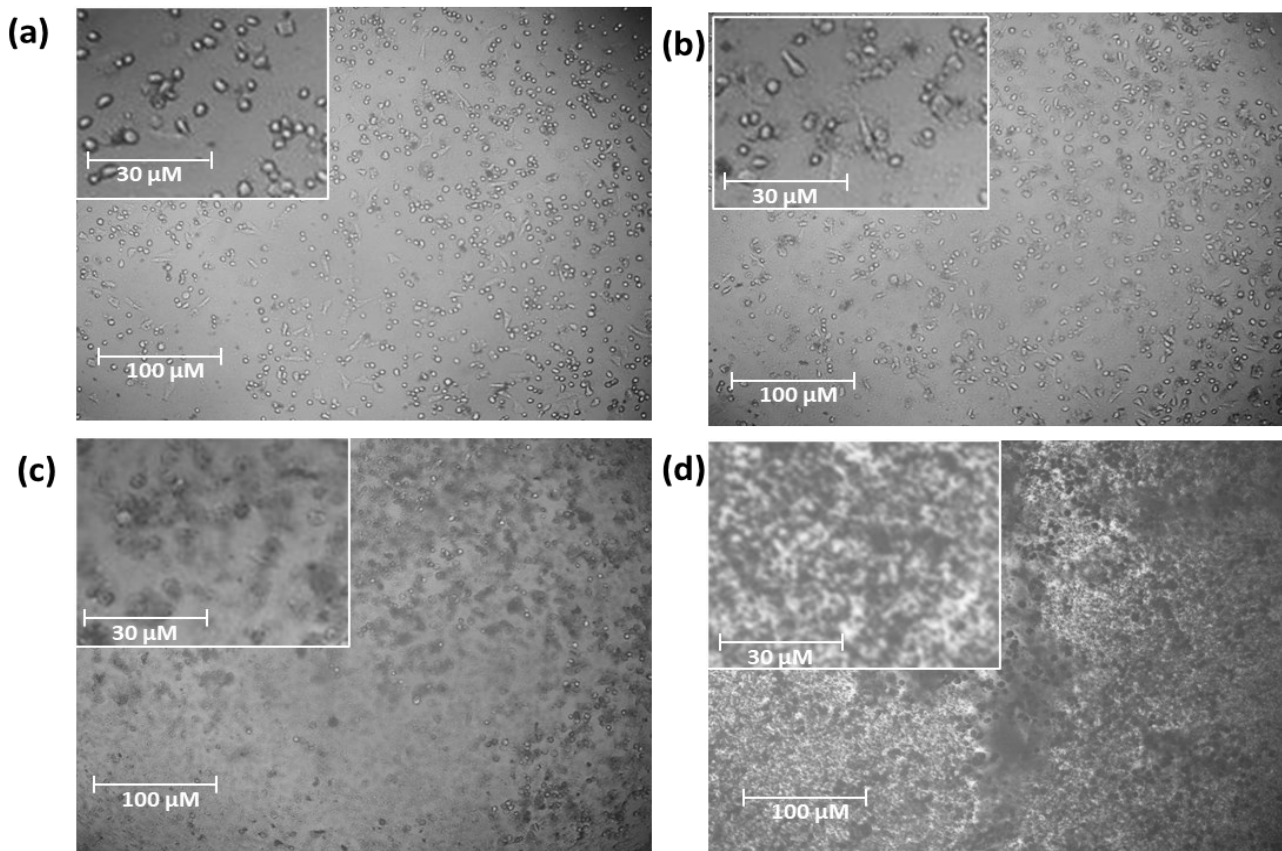


Fig. 9. Microscopic images of HeLa cells treated with MSN^{MPA/SirP} (a) First one hour of treatment improper settlement of the cells (b) 12 hours of treatment cells started to deformation of the shape (c) 24 hours of treatment bleeding of the cell membrane followed by detachment (d) 48 hours of treatment with aggregation of dead cells, insight images are magnified for cellular observations

cytotoxicity of the MSN^{MPA/SirP} complex compared to free SirP suggests improved delivery and potential increased cellular uptake, highlighting the utility of nanoparticles as drug carriers. The visible morphological changes further validated our cytotoxicity findings as shown in Fig. 9(c) and 9(d). The observed cellular aggregation and membrane damage are indicative of apoptosis initiation, a common mechanism of action for several anticancer drugs. The present results underscore the promise of MSN^{MPA/SirP} complexes in anticancer treatment. The alignment between cytotoxicity and morphological data bolsters this proposition, warranting further exploration and validation in subsequent studies.

Conclusion

This study demonstrated the synthesis, purification, and analysis of crude SirP proteins and their binding to mesoporous silica nanoparticles. The confirmation of MSN^N synthesis was achieved by a range of techniques, including TEM, SEM, XRD, AFM, and DLS. These techniques were employed to verify the size, shape, and stability of the nanoparticles. The validation of the bioconjugation between MSN and SirP was confirmed by observing changes in zeta potential and the presence of unique FTIR peaks. The cytotoxicity experiments demonstrated that MSN^N alone did not substantially affect HeLa cells. However, the SirP-conjugated MSN^{MPA/SirP} exhibited noteworthy anticancer activity, with an IC₅₀ value of 10 µg/mL. This suggests the potential of MSN as an efficient vehicle for protein delivery in cancer treatment. The findings are consistent with other studies, providing new opportunities for the development of cutting-edge nanotechnology-based treatments for cancer.

Supplementary information

The determination of protein concentration (a) Standard graph of bovine serum albumin (BSA) with mean optical densities (b) Estimated protein concentration of SirP in various broth cultures is mentioned in Fig. S1. The author(s) is responsible for the content or functionality of any supplementary information. Any queries regarding the same should be directed to the corresponding author. The supplementary information is downloadable from the article's webpage and will not be printed in the print copy.

Ethical statement

None of the animal or human samples were used in this research.

Conflict of interest

The authors declare that they have no conflict of interest.

REFERENCES

- Ahmadi, F., A. Sodagar-Taleghani, P. Ebrahimnejad, S. P. H. Moghaddam, F. Ebrahimnejad, K. Asare-Addo & A. Nokhodchi (2022) A review on the latest developments of mesoporous silica nanoparticles as a promising platform for diagnosis and treatment of cancer. *International Journal of Pharmaceutics*, 122099. <https://doi.org/10.1016/j.ijpharm.2022.122099>
- Albalawi, F., M. Z. Hussein, S. Fakurazi & M. J. Masarudin (2021) Engineered nanomaterials: The challenges and opportunities for nanomedicines. *International journal of nanomedicine*, 161-184. <https://doi.org/10.2147/IJN.S288236>
- Anchordoquy, T. J., Y. Barenholz, D. Boraschi, M. Chorny, P. Decuzzi, M. A. Dobrovolskaia, Z. S. Farhangrazi, D. Farrell, A. Gabizon & H. Ghandehari. 2017. Mechanisms and barriers in cancer nanomedicine: addressing challenges, looking for solutions. ACS Publications. <https://doi.org/10.1021/acsnano.6b08244>
- Asefa, T. & Z. Tao (2012) Biocompatibility of mesoporous silica nanoparticles. *Chemical research in toxicology*, 25, 2265-2284. <https://doi.org/10.1021/tx300166u>
- Barrow, P. (2007) Salmonella infections: immune and non-immune protection with vaccines. *Avian pathology*, 36, 1-13. <https://doi.org/10.1080/03079450601113167>
- Bernal-Bayard, J., E. Cardenal-Munoz & F. Ramos-Morales (2010) The Salmonella type III secretion effector, salmonella leucine-rich repeat protein (SirP), targets the human chaperone ERdj3. *Journal of Biological Chemistry*, 285, 16360-16368. <https://doi.org/10.1074/jbc.M110.100669>
- Braun, K., C. M. Stürzel, J. Biskupek, U. Kaiser, F. Kirchoff & M. Lindén (2018) Comparison of different cytotoxicity assays for in vitro evaluation of mesoporous silica nanoparticles. *Toxicology in Vitro*, 52, 214-221. <https://doi.org/10.1016/j.tiv.2018.06.019>
- Bray, F., J. Ferlay, I. Soerjomataram, R. L. Siegel, L. A. Torre & A. Jemal (2018) Global cancer statistics 2018: GLOBOCAN estimates of incidence and mortality worldwide for 36 cancers in 185 countries. *CA: a cancer journal for clinicians*, 68, 394-424. <https://doi.org/10.3322/caac.21492>
- Cani, P. D. (2018) Human gut microbiome: hopes, threats and promises. *Gut*, 67, 1716-1725. <https://doi.org/10.1136/gutjnl-2018-316723>
- Chenthamara, D., S. Subramaniam, S. G. Ramakrishnan, S. Krishnaswamy, M. M. Essa, F.-H. Lin & M. W. Qoronfleh (2019) Therapeutic efficacy of nanoparticles and routes of administration. *Biomaterials Research*, 23, 1-29. <https://doi.org/10.1186/s40824-019-0166-x>
- Cheng Y. J., Ai-Qing Z., Jing-Jing H., Feng H., Xuan Z., and Xian-Zheng Z (2017) Multifunctional peptide-amphiphile end-capped mesoporous silica nanoparticles for tumor targeting drug delivery. *ACS applied materials & interfaces*, 9, 2093-2103. <https://doi.org/10.1021/acsaami.6b12647>
- Cordero-Alba, M. & F. Ramos-Morales (2014) Patterns of expression and translocation of the ubiquitin ligase SirP in Salmonella enterica serovar Typhimurium. *Journal of bacteriology*, 196, 3912-3922. <https://doi.org/10.1128/jb.02158-14>

13. Costas, M. (1995) The analysis of bacterial proteins by SDS polyacrylamide gel electrophoresis. *Diagnostic Bacteriology Protocols*, 27-40.
14. Cubillos-Ruiz, A., T. Guo, A. Sokolovska, P. F. Miller, J. J. Collins, T. K. Lu & J. M. Lora (2021) Engineering living therapeutics with synthetic biology. *Nature Reviews Drug Discovery*, 20, 941-960. <https://doi.org/10.1385/0-89603-297-3:27>
15. Dailey, K. M., J. E. Allgood, P. R. Johnson, M. A. Ostlie, K. C. Schaner, B. D. Brooks & A. E. Brooks (2021) The next frontier of oncotherapy: accomplishing clinical translation of oncolytic bacteria through genetic engineering. *Future Microbiology*, 16, 341-368. <https://doi.org/10.2217/fmb-2020-0245>
16. Di Pasqua, A. J., K. K. Sharma, Y.-L. Shi, B. B. Toms, W. Ouellette, J. C. Dabrowiak & T. Asefa (2008) Cytotoxicity of mesoporous silica nanomaterials. *Journal of inorganic biochemistry*, 102, 1416-1423. <https://doi.org/10.1016/j.jinorgbio.2007.12.028>
17. Dzutsev, A., J. H. Badger, E. Perez-Chanona, S. Roy, R. Salcedo, C. K. Smith & G. Trinchieri (2017) Microbes and cancer. *Annual review of immunology*, 35, 199-228. <https://doi.org/10.1146/annurev-immunol-051116-052133>
18. Ehrbar, K., A. Friebel, S. I. Miller & W.-D. Hardt (2003) Role of the Salmonella pathogenicity island 1 (SPI-1) protein InvB in type III secretion of SopE and SopE2, two Salmonella effector proteins encoded outside of SPI-1. *Journal of bacteriology*, 185, 6950-6967. <https://doi.org/10.1128/JB.185.23.6950-6967.2003>
19. Farjadian, F., A. Roointan, S. Mohammadi-Samani & M. Hosseini (2019) Mesoporous silica nanoparticles: synthesis, pharmaceutical applications, biodistribution, and biosafety assessment. *Chemical Engineering Journal*, 359, 684-705. <https://doi.org/10.1016/j.cej.2018.11.156>
20. Figueroa-Bossi, N., S. Uzzau, D. Malorli & L. Bossi (2001) Variable assortment of prophages provides a transferable repertoire of pathogenic determinants in Salmonella. *Molecular microbiology*, 39, 260-272. <https://doi.org/10.1046/j.1365-2958.2001.02234.x>
21. Florek, J., R. Caillard & F. Kleitz (2017) Evaluation of mesoporous silica nanoparticles for oral drug delivery—current status and perspective of MSNs drug carriers. *Nanoscale*, 9, 15252-15277. <https://doi.org/10.1039/C7NR05762H>
22. Forbes, N. S. (2010) Engineering the perfect (bacterial) cancer therapy. *Nature Reviews Cancer*, 10, 785-794. <https://doi.org/10.1038/nrc2934>
23. Frickenstein, A. N., J. M. Hagood, C. N. Britten, B. S. Abbott, M. W. McNally, C. A. Vopat, E. G. Patterson, W. M. MacCuaig, A. Jain & K. B. Walters (2021) Mesoporous silica nanoparticles: Properties and strategies for enhancing clinical effect. *Pharmaceutics*, 13, 570. <https://doi.org/10.3390/pharmaceutics13040570>
24. Gao, F., Y. Liu, C. Lei, C. Liu, H. Song, Z. Gu, P. Jiang, S. Jing, J. Wan & C. Yu (2021) The role of dendritic mesoporous silica nanoparticles' size for quantum dots enrichment and lateral flow immunoassay performance. *Small Methods*, 5, 2000924. <https://doi.org/10.1002/smt.202000924>
25. Gu, L., A. Zhang, K. Hou, C. Dai, S. Zhang, M. Liu, C. Song & X. Guo (2012) One-pot hydrothermal synthesis of mesoporous silica nanoparticles using formaldehyde as growth suppressant. *Microporous and Mesoporous Materials*, 152, 9-15. <https://doi.org/10.1016/j.micromeso.2011.11.047>
26. Guirnalda, P., L. Wood, M. Seavey & Y. Paterson (2012) Intracellular Facultative Bacterial Vectors for Cancer Immunotherapy. *Vaccinology: Principles and Practice*, 255-274. <https://doi.org/10.1002/9781118345313.ch17>
27. Haraga, A. 2005. *Study of the intracellular function of the Salmonella enterica serovar Typhimurium type III secretion effector SspH1*. University of Washington. <https://doi.org/10.1111/j.1462-5822.2005.00670.x>
28. Hossen, S., M. K. Hossain, M. Basher, M. Mia, M. Rahman & M. J. Uddin (2019) Smart nanocarrier-based drug delivery systems for cancer therapy and toxicity studies: A review. *Journal of advanced research*, 15, 1-18. <https://doi.org/10.1016/j.jare.2018.06.005>
29. Huang, X., J. Pan, F. Xu, B. Shao, Y. Wang, X. Guo & S. Zhou (2021) Bacteria-based cancer immunotherapy. *Advanced Science*, 8, 2003572. <https://doi.org/10.1002/advs.202003572>
30. Hurley, D., M. P. McCusker, S. Fanning & M. Martins (2014) Salmonella–host interactions—modulation of the host innate immune system. *Frontiers in immunology*, 5, 481. <https://doi.org/10.3389/fimmu.2014.00481>
31. Jafari, M., B. Zargar, M. Soltani, D. N. Karunaratne, B. Ingalls & P. Chen (2012) Intelligent drug delivery systems for cancer therapy. *Biomedical Materials and Diagnostic Devices*, 477-513. <https://doi.org/10.1002/9781118523025.ch15>
32. Jafari, S., H. Derakhshankhah, L. Alaei, A. Fattahi, B. S. Varnamkhasti & A. A. Saboury (2019) Mesoporous silica nanoparticles for therapeutic/diagnostic applications. *Biomedicine & Pharmacotherapy*, 109, 1100-1111. <https://doi.org/10.1016/j.biopha.2018.10.167>
33. Kaasalainen, M., V. Aseyev, E. von Haartman, D. Ş. Karaman, E. Mäkilä, H. Tenhu, J. Rosenholm & J. Salonen (2017) Size, stability, and porosity of mesoporous nanoparticles characterized with light scattering. *Nanoscale research letters*, 12, 1-10. <https://doi.org/10.1186/s11671-017-1853-y>
34. Kalia, V. C., S. K. Patel, B.-K. Cho, T. K. Wood & J.-K. Lee. 2022. Emerging applications of bacteria as antitumor agents. In *Seminars in Cancer Biology*, 1014-1025. Elsevier. <https://doi.org/10.1016/j.semcancer.2021.05.012>
35. Kankala, R. K., H. Zhang, C. G. Liu, K. R. Kanubaddi, C. H. Lee, S. B. Wang, W. Cui, H. A. Santos, K. Lin & A. Z. Chen (2019) Metal species-encapsulated mesoporous silica nanoparticles: current advancements and latest breakthroughs. *Advanced Functional Materials*, 29, 1902652. <https://doi.org/10.1002/adfm.201902652>
36. Keshavarz, M. & N. Ahmad (2013) Characterization and modification of mesoporous silica nanoparticles prepared by sol-gel. *Journal of Nanoparticles*, 2013. <https://doi.org/10.1155/2013/102823>
37. Kobler, J., K. Möller & T. Bein (2008) Colloidal suspensions of functionalized mesoporous silica nanoparticles. *ACS nano*, 2, 791-799. <https://doi.org/10.1021/nn700008s>
38. Kuznetsov, M., J. Clairambault & V. Volpert (2021) Improving cancer treatments via dynamical biophysical models. *Physics of life reviews*, 39, 1-48. <https://doi.org/10.1016/j.plrev.2021.10.001>
39. Layton, A. N. & E. E. Galyov (2007) Salmonella-induced enteritis: molecular pathogenesis and therapeutic implications.

- tions. *Expert Reviews in Molecular Medicine*, 9, 1-17. <https://doi.org/10.1017/S1462399407000373>
40. Leschner, S., K. Westphal, N. Dietrich, N. Viegas, J. Jablonska, M. Lyszkiewicz, S. Lienenklaus, W. Falk, N. Gekara & H. Loessner (2009) Tumor invasion of Salmonella enterica serovar Typhimurium is accompanied by strong hemorrhage promoted by TNF- α . *PLoS one*, 4, e6692. <https://doi.org/10.1371/journal.pone.0006692>
 41. Liang, K., Q. Liu, P. Li, H. Luo, H. Wang & Q. Kong (2019) Genetically engineered Salmonella Typhimurium: Recent advances in cancer therapy. *Cancer letters*, 448, 168-181. <https://doi.org/10.1016/j.canlet.2019.01.037>
 42. Lin, C.-Y., C.-M. Yang & M. Lindén (2019) Influence of serum concentration and surface functionalization on the protein adsorption to mesoporous silica nanoparticles. *RSC advances*, 9, 33912-33921. DOI <https://doi.org/10.1039/C9RA05585A>
 43. Liu, X., F. Wu, Y. Ji & L. Yin (2018) Recent advances in anti-cancer protein/peptide delivery. *Bioconjugate chemistry*, 30, 305-324. <https://doi.org/10.1021/acs.bioconjchem.8b00750>
 44. Lu, Y.-Y. 2015. Modulation of host immune responses by Bartonella effector proteins. University_of_Basel.
 45. Lugano, R., M. Ramachandran & A. Dimberg (2020) Tumor angiogenesis: causes, consequences, challenges and opportunities. *Cellular and Molecular Life Sciences*, 77, 1745-1770. <https://doi.org/10.1007/s00018-019-03351-7>
 46. Maggini, L., I. Cabrera, A. Ruiz-Carretero, E. A. Prasetyanto, E. Robinet & L. De Cola (2016) Breakable mesoporous silica nanoparticles for targeted drug delivery. *Nanoscale*, 8, 7240-7247. <https://doi.org/10.1039/C5NR09112H>
 47. Manzano, M. & M. Vallet-Regí (2020) Mesoporous silica nanoparticles for drug delivery. *Advanced functional materials*, 30, 1902634. <https://doi.org/10.1002/adfm.201902634>
 48. Martín, M. J., F. Lara-Villoslada, M. A. Ruiz & M. E. Morales (2015) Microencapsulation of bacteria: A review of different technologies and their impact on the probiotic effects. *Innovative Food Science & Emerging Technologies*, 27, 15-25. <https://doi.org/10.1016/j.ifset.2014.09.010>
 49. Mohseni, M., K. Gilani & S. A. Mortazavi (2015) Preparation and characterization of rifampin loaded mesoporous silica nanoparticles as a potential system for pulmonary drug delivery. *Iranian journal of pharmaceutical research: IJPR*, 14, 27.
 50. Nuti, R., N. S. Goud, A. P. Saraswati, R. Alvala & M. Alvala (2017) Antimicrobial peptides: a promising therapeutic strategy in tackling antimicrobial resistance. *Current medicinal chemistry*, 24, 4303-4314. <https://doi.org/10.2174/0929867324666170815102441>
 51. Parasuraman, P., A. P. Antony, A. Sharan, B. Siddhardha, K. Kasinathan, N. A. Bahkali, T. M. Dawoud & A. Syed (2019) Antimicrobial photodynamic activity of toluidine blue encapsulated in mesoporous silica nanoparticles against Pseudomonas aeruginosa and Staphylococcus aureus. *Biofouling*, 35, 89-103. <https://doi.org/10.1080/08927014.2019.1570501>
 52. Pucci, C., C. Martinelli & G. Ciofani (2019) Innovative approaches for cancer treatment: Current perspectives and new challenges. *ecancermedicalscience*, 13. <https://doi.org/10.3332/ecancer.2019.961>
 53. Rameli, N., K. Jumbri, R. Wahab, A. Ramli & F. Huyop. 2018. Synthesis and characterization of mesoporous silica nanoparticles using ionic liquids as a template. In *Journal of Physics: Conference Series*, 012068. IOP Publishing. <https://doi.org/10.1088/1742-6596/1123/1/012068>
 54. Ramos-Morales, F. (2012) Impact of Salmonella enterica type III secretion system effectors on the eukaryotic host cell. *International Scholarly Research Notices*, 2012. <https://doi.org/10.5402/2012/787934>
 55. Rook, G. A. & A. Dalgleish (2011) Infection, immunoregulation, and cancer. *Immunological reviews*, 240, 141-159. <https://doi.org/10.1111/j.1600-065X.2010.00987.x>
 56. Roy, S. & G. Trinchieri (2017) Microbiota: a key orchestrator of cancer therapy. *Nature Reviews Cancer*, 17, 271-285. <https://doi.org/10.1038/nrc.2017.13>
 57. Sedighi, M., A. Zahedi Bialvaei, M. R. Hamblin, E. Ohadi, A. Asadi, M. Halajzadeh, V. Lohrasbi, N. Mohammadzadeh, T. Amirani & M. Krutova (2019) Therapeutic bacteria to combat cancer; current advances, challenges, and opportunities. *Cancer medicine*, 8, 3167-3181. <https://doi.org/10.1002/cam4.2148>
 58. Shelburne, N., B. Adhikari, J. Brell, M. Davis, P. Desvigne-Nickens, A. Freedman, L. Minasian, T. Force & S. C. Remick (2014) Cancer treatment-related cardiotoxicity: current state of knowledge and future research priorities. *Journal of the National Cancer Institute*, 106, dju232. <https://doi.org/10.1093/jnci/dju232>
 59. Tang, F., L. Li & D. Chen (2012) Mesoporous silica nanoparticles: synthesis, biocompatibility and drug delivery. *Advanced materials*, 24, 1504-1534. <https://doi.org/10.1002/adma.201104763>
 60. Toussaint, B., X. Chauchet, Y. Wang, B. Polack & A. L. Gouëllec (2013) Live-attenuated bacteria as a cancer vaccine vector. *Expert review of vaccines*, 12, 1139-1154. <https://doi.org/10.1586/14760584.2013.836914>
 61. Tsakalidou, E., E. Manolopoulou, E. Kabarakis, E. Zoidou, B. Pot, K. Kersters & G. Kalantzopoulos (1994) The combined use of whole-cell protein extracts for the identification (SDS-PAGE) and enzyme activity screening of lactic acid bacteria isolated from traditional Greek dairy products. *Systematic and Applied Microbiology*, 17, 444-458. [https://doi.org/10.1016/S0723-2020\(11\)80062-7](https://doi.org/10.1016/S0723-2020(11)80062-7)
 62. Van Mellaert, L., S. Barbé & J. Anné (2006) Clostridium spores as anti-tumour agents. *TRENDS in Microbiology*, 14, 190-196. <https://doi.org/10.1016/j.tim.2006.02.002>
 63. Vyshnava, S. S., D. K. Kanderi & M. R. Dowlatabad (2022a) Confocal laser scanning microscopy study of intercellular events in filopodia using 3-mercaptopropionic acid capped CdSe/ZnS quantum dots. *Micron*, 153, 103200. <https://doi.org/10.1016/j.micron.2021.103200>
 64. Vyshnava, S. S., G. Pandluru, D. K. Kanderi, S. P. Panjala, S. Banapuram, K. Paramasivam, R. R. Anupalli, R. R. Bontha & M. R. Dowlatabad (2020) Gram scale synthesis of QD 450 core-shell quantum dots for cellular imaging and sorting. *Applied Nanoscience*, 10, 1257-1268. <https://doi.org/10.1007/s13204-020-01261-w>
 65. Vyshnava, S. S., G. Pandluru, K. D. Kumar, S. P. Panjala, S. Banapuram, K. Paramasivam, K. V. Devi, R. R. Anupalli & M. R. Dowlatabad (2022b) Quantum dots based in-vitro co-culture cancer model for identification of rare cancer

- cell heterogeneity. *Scientific Reports*, 12, 5868. <https://doi.org/10.1038/s41598-022-09702-y>
66. Vyshnava, S. S., G. Pandluru, K. D. Kumar, S. P. Panjala, K. Paramasivam, S. Banapuram, R. R. Anupalli & M. R. Dowlatabad (2022c) Biocompatible Ni-doped CdSe/ZnS semiconductor nanocrystals for cellular imaging and sorting. *Luminescence*, 37, 490-499. <https://doi.org/10.1002/bio.4199>
67. Wang, Y., N. Han, Q. Zhao, L. Bai, J. Li, T. Jiang & S. Wang (2015) Redox-responsive mesoporous silica as carriers for controlled drug delivery: a comparative study based on silica and PEG gatekeepers. *European journal of pharmaceutical sciences*, 72, 12-20. <https://doi.org/10.1016/j.ejps.2015.02.008>
68. Wei, M. Q., A. Mengesha, D. Good & J. Anné (2008) Bacterial targeted tumour therapy-dawn of a new era. *Cancer letters*, 259, 16-27. <https://doi.org/10.1016/j.canlet.2007.10.034>
69. Wong, S. H. & J. Yu (2019) Gut microbiota in colorectal cancer: mechanisms of action and clinical applications. *Nature Reviews Gastroenterology & Hepatology*, 16, 690-704. <https://doi.org/10.1038/s41575-019-0209-8>
70. Zargar, B. (2014) A Synthetic Biology Approach to Bacteria Mediated Tumor Targeting.
71. Zhang, J., X. Li, J. M. Rosenholm & H.-c. Gu (2011) Synthesis and characterization of pore size-tunable magnetic mesoporous silica nanoparticles. *Journal of colloid and interface science*, 361, 16-24. <https://doi.org/10.1016/j.jcis.2011.05.038>
72. Zouhir, S., J. Bernal-Bayard, M. Cordero-Alba, E. Cardenal-Munoz, B. Guimaraes, N. Lazar, F. Ramos-Morales & S. Nessler (2014) The structure of the Slrp-Trx1 complex sheds light on the autoinhibition mechanism of the type III secretion system effectors of the NEL family. *Biochemical Journal*, 464, 135-144. <https://doi.org/10.1042/BJ20140587>
73. Zugazagoitia, J., C. Guedes, S. Ponce, I. Ferrer, S. Molina-Pinelo & L. Paz-Ares (2016) Current challenges in cancer treatment. *Clinical therapeutics*, 38, 1551-1566. <https://doi.org/10.1016/j.clinthera.2016.03.026>
74. Zygouropoulou, M., A. Kubiak, A. V. Patterson & N. P. Minton (2019) Genetic Engineering of Clostridial Strains for Cancer Therapy. *Microbial Infections and Cancer Therapy*, <https://doi.org/10.1201/9781351041904-3>